Available online at www.sciencedirect.com
SCIENCE DIRECT
International Journal of Heat and Mass Transfer 49 (2006) 2673–2683
International Journal of HEAT and MASS TRANSFER
www.elsevier.com/locate/ijhmt

Fuel cell entropy production with ohmic heating and diffusive polarization

G.F. Naterer [a,*], C.D. Tokarz [b], J. Avsec [c]

[a] Faculty of Engineering and Applied Science, University of Ontario Institute of Technology, 2000 Simcoe Street N, Oshawa, Ont., Canada L1H 7K4
[b] Department of Mechanical and Manufacturing Engineering, University of Manitoba, 15 Gillson Street, Winnipeg, Manitoba, Canada R3T 2N2
[c] Faculty of Mechanical Engineering, University of Maribor, Smetanova 17, 2000 Maribor, Slovenia

Received 14 August 2005; received in revised form 9 January 2006
Available online 9 March 2006

Abstract

In this article, entropy production of ohmic heating and concentration polarization is investigated for two types of fuel cells (PEMFC and SOFC). Ohmic entropy production arises from resistance to electron flow through the electrodes, as well as ion flow through the electrolyte. Ohm's law is applied to both ion and electron flows, when formulating the entropy production. Also, entropy production arises from changes in concentration of the reactants, during fuel consumption at the electrode surfaces. Unlike past methods developed for a solid oxide fuel cell (SOFC), this article formulates entropy production within electrodes of a proton exchange membrane fuel cell (PEMFC). Predicted results of cell irreversibilities are successfully validated against measured data. The entropy based method provides a useful alternative to past schemes aiming to reduce voltage losses with polarization curves, as entropy production is directly governed by the Second Law and it encompasses both electrochemical and thermofluid irreversibilities within a fuel cell.

Keywords: Fuel cell; Entropy production; Ohmic heating

1. Introduction

Fuel cells represent a promising future alternative to internal combustion engines for vehicle transportation. But a key challenge for fuel cells is their overall efficiency. Bossel [1] has reported that a "power plant to wheel efficiency" of about 22% was calculated for typical operating conditions of a PEMFC, compared with advanced diesel (25%) and hybrid electric with SOFC range extension (33%). This article investigates thermochemical processes of entropy production in fuel cells, in efforts to develop an alternative entropy based method for systematically improving efficiency of fuel cells.

In addition to relatively low efficiencies, a key challenge of automotive fuel cells is quick start-up capabilities in cold weather conditions. After shutdown of a fuel cell, water freezes in a PEMFC at sub-zero temperatures. Oszcipok et al. [2] have investigated cold startup behavior of fuel cells, particularly with respect to charge transfer through the membrane and water production. Charge transfer curves were obtained statistically in cold startup conditions. A unique difficulty of predicting heat transfer during freezing of water is the unknown position of the moving solid/liquid interface [3,4]. It was reported that the initial starting electric current depends on the membrane humidity and operational voltage. The decay of electrical current depends on the flow rate of reactant gases. Based on cyclic voltammetry and polarization curves from impedance spectra measurements at freezing temperatures, Oszcipok et al. [2] have reported that ice formation in the porous structures leads to significant performance losses in a fuel cell. In this article, voltage losses of a PEMFC are characterized with respect to entropy production, which can include the latent entropy of fusion to accommodate entropy transport with freezing of water [5,6].

* Corresponding author. Tel.: +1 9057213111/2810; fax: +1 9057213370.
E-mail address: greg.naterer@uoit.ca (G.F. Naterer).

0017-9310/$ - see front matter © 2006 Elsevier Ltd. All rights reserved.
doi:10.1016/j.ijheatmasstransfer.2006.01.009

Nomenclature

C	concentration (mol/m^3)
C_l	membrane molar liquid content (mol/m^3)
D	diffusion coefficient (m^2/s)
E	voltage (V)
E^0	standard equilibrium potential (V)
F	Faraday's constant (96,785 C/mol)
i	current density (A/m^2)
J	flux (mol/s)
K	equilibrium constant
l	thickness (m)
n_d	electro-osmotic drag coefficient
n_e	moles of electrons per half-cell reaction
N	number of moles per mole H_2
P	pressure (Pa)
P_s	entropy production rate (J/mol K)
$\bar{r}$	average pore radius (m)
R	universal gas constant (8.314 J/mol K)
S_A	specific area of electrode (m^2/kg)
T	temperature (K)
v	velocity (m/s)
X	mole fraction

Greek symbols

δ	diffusion ratio
ε	porosity
η	polarization (V)
Ω_D	Lennard–Jones potential
ρ	density (kg/m^3)
σ	collision diameter (A)
σ_m	ionic conductivity (1/Ω m)
ξ	tortuosity

Subscripts

a	anode
A, B	components A, B
c	cathode
eff	effective
H^+	hydrogen ion
H_2	hydrogen
H_2O	water vapor
k	Knudsen coefficient
m	membrane/electrolyte
O_2	oxygen
0	exchange

This article focuses on diffusive and ohmic entropy production in fuel cells. Ohmic losses were measured experimentally in a PEMFC with a current interruption method by Mennola et al. [7]. Voltage transients were monitored with a digital oscilloscope connected to an individual cell. Results indicated that ohmic losses increased by up to 21% at 400 mA/cm^2 at the highest air flow rates, due to drying and a lower membrane conductivity. This article investigates how ohmic heating contributes to the overall entropy production within a PEMFC and SOFC.

Fuel channels blocked with baffles to enhance gas transport were studied numerically by Liu et al. [8]. It was proposed that additional fuel could be transported into the gas diffusion layer with baffle blockage, so chemical reactions would be enhanced to improve fuel cell performance. The results have shown that gas transport and current generation were enhanced by the baffles. But baffles enhance mixing at the expense of higher losses of pressure in the fuel channels, which entail added input power of blowers. Entropy production provides a useful parameter for effectively balancing these losses against higher power output of the fuel cell.

A serpentine path between fuel channels in a PEMFC was studied numerically by Dutta et al. [9]. Mass consumption in a membrane electrode assembly (MEA) affected flow distributions in both anode and cathode side channels. Unlike straight channels, higher pressure drops were reported by the authors for serpentine paths. In addition to different paths, varying cross-sectional profiles of channels affect the wall friction, including possible transition to slip-flow conditions in microchannels. Naterer [10] has reported that surface microchannels with varying cross-sectional profiles reduce exergy losses in convective heat transfer, due to slip-flow drag reduction within the microchannels.

Detailed analysis of non-isothermal and non-isobaric transport in a PEMFC was studied by Djilali and Lu [11]. The formulation was solved numerically to predict diffusion through the porous electrodes, as well as ohmic heating and coupled convective/electro-osmotic transport of liquid water in the electrodes. The reaction kinetics was predicted with the Butler–Volmer equation. Their formulation considered hydrodynamics within small pores in the porous electrodes. Ohmic and diffusive mechanisms are also considered in this article, but with detailed focus regarding their effects on entropy production within a fuel cell.

A vorticity/velocity method and power law scheme were developed by Jen et al. [12] to predict 3-D transport within fuel channels and electrodes of a PEMFC. Close agreement between numerical predictions and measured data was reported. Both axial and secondary flow fields were predicted numerically. Polarization distributions were determined based on electrochemical reactions and membrane phase potentials predicted with the numerical scheme. In

contrast, this article determines electrochemical polarization within a fuel cell using entropy production and the Second Law.

Chan and Xia [13] have reported effects of ohmic, activation and concentration polarization on performance of solid oxide fuel cells. In contrast to an SOFC, this article extends past studies of entropy production to a PEMFC. This requires different half-cell reactions, operating conditions and diffusive coefficients when deriving expressions for the entropy production. Chan and Xia [13] have determined SOFC heat losses from an entropy balance. A Butler–Volmer model of activation polarization was developed by the authors. Both ordinary diffusion and Knudsen diffusion rates were considered in the concentration polarization. The concentration resistance at the anode was reduced after hydrogen was humidified sufficiently.

Various other correlations for predicting irreversibilities and voltage losses in fuel cells were investigated by Ghadamian and Saboohi [14]. Activation, fuel cross-over, concentration and ohmic losses were formulated by the authors. Then, the accumulated voltage losses were subtracted from the open circuit voltage to predict the operating voltage. In contrast, this article derives models of ohmic resistance and diffusive mass transfer, when formulating expressions for the entropy production. More generally, this article aims to develop an alternative entropy based method of systematically improving performance of fuel cells.

2. Entropy production of ohmic heating

A PEMFC converts chemical energy of oxidant (oxygen) and fuel (hydrogen) streams into electricity through an electrochemical reaction (see Fig. 1). The energy conversion provides continuous power to an electrical circuit, provided that oxidant and fuel streams are supplied. Ohmic voltage losses arise from resistance to electron flow through the electrodes, as well as ion flow through the electrolyte. The electrical resistance to ion/electron flow obeys Ohm's law, so the ohmic polarization can be written as

$$\eta_{\text{ohm}} = i \cdot (R_{\text{m}} + R_{\text{ohm,a}} + R_{\text{ohm,c}}) \tag{1}$$

The dominant voltage losses usually occur through the electrolyte (subscript m). The ohmic resistance through the anode and cathode ($R_{\text{ohm,a}}$ and $R_{\text{ohm,c}}$) will be assumed as negligible.

Electrolyte resistance depends on the water content of the membrane. If the membrane was perfectly humidified, the limiting current would arise from imperfect oxygen transport through the electrodes (called the concentration polarization). The limiting current density refers to the current density when the cell voltage potential becomes zero. Without complete humidification, the limiting current depends on processes of membrane drying. Humidification of the membrane changes due to back diffusion of water from the cathode side of the fuel cell into the membrane. The membrane resistance and ohmic losses increase with larger differences between ideal (perfect) and actual humidification.

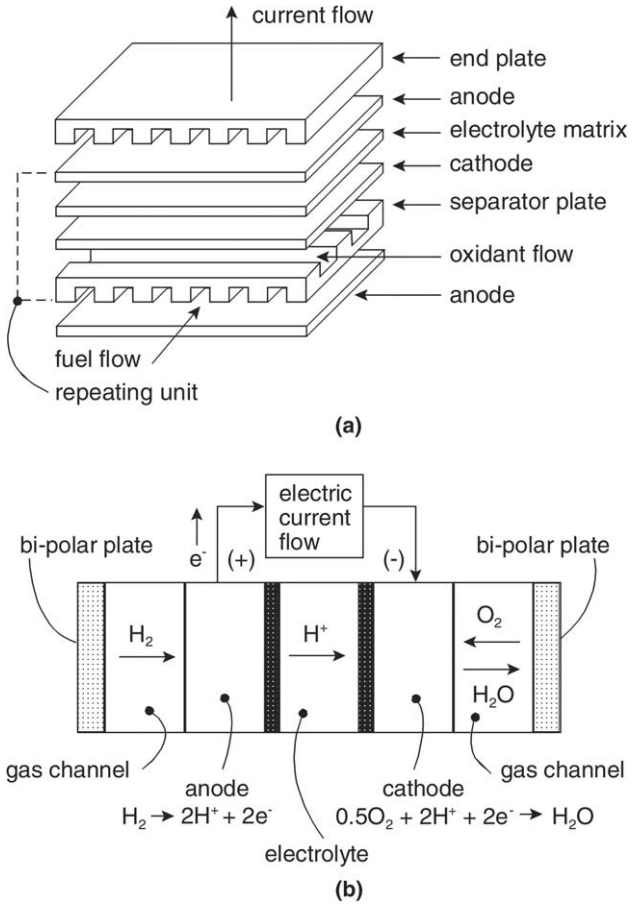

Fig. 1. Schematic of a proton exchange membrane fuel cell.

Consider 1-D mass diffusion within the electrolyte, with $x = 0$ at the anode/electrolyte interface. The ohmic resistance can be expressed as follows:

$$\eta_{\text{ohm,m}} = iR_{\text{m}} = i \int_0^{l_{\text{m}}} \frac{\mathrm{d}x}{\sigma_{\text{m}}(x)} \tag{2}$$

In this equation, σ_{m} refers to the membrane ionic conductivity, which can be calculated based on [13]

$$\sigma_{\text{m}}(x) = \sigma_{\text{m0}} \frac{C_{\text{l}}(x)}{C_{\text{H}^+}} \tag{3}$$

where C_{l} is the membrane molar concentration of liquid water (mol/cm^3), C_{H^+} is the membrane molar concentration of protons (mol/cm^3) and σ_{m0} is the ionic conductivity at unit water content.

The fuel cell operating temperature is assumed to be sufficiently high, so that liquid water transport within the solid electrode can be neglected. Also, when the electro-osmotic flux (proton transfer) and back diffusion of water vapour are equal, it can be shown that

$$D_{\text{m}} \frac{\mathrm{d}C_{\text{l}}}{\mathrm{d}x} = n_{\text{d}} \frac{i}{F} \tag{4}$$

where n_{d} is the electro-osmotic drag coefficient. Then, integrating Eq. (4) over the thickness of the membrane yields

$$\int_{C_{l,a}}^{C_{l,c}} dC_l = \int_0^{l_m} \frac{n_d i}{D_m F} dx \tag{5}$$

which becomes

$$C_{l,a} = C_{l,c} - \frac{n_d i}{D_m F} l_m \tag{6}$$

The result in Eq. (6) represents a molar concentration at the anode/electrolyte interface. Since the diffusive flux is proportional to the molar concentration, Ohm's law requires that the molar concentration increases linearly across the membrane, from the previous result in Eq. (6) at the anode to $C_{l,c}$ at the cathode. Therefore,

$$C_l(x) = \frac{n_d i}{D_m F} x + \left(C_{l,c} - \frac{n_d l_m i}{D_m F} \right) \tag{7}$$

Alternatively,

$$C_l(x) = C_{l,c} \left[1 + \frac{i}{i_L} \cdot \left(\frac{x}{l_m} - 1 \right) \right] \tag{8}$$

where

$$i_L = \frac{F D_m C_{l,c}}{n_d l_m} \tag{9}$$

It can be observed that $C_l(0) = 0$ when $i = i_L$ or the membrane is dry. This case of $i = i_L$ represents the limiting current within the fuel cell.

Substituting Eq. (9) into Eq. (2) gives

$$\eta_{ohm,m} = i \int_0^{l_m} \left[\frac{C_{H^+}}{C_{l,c}} \Big/ \left(1 + \frac{i}{i_L} \left(\frac{x}{l_m} - 1 \right) \right) \right] dx \tag{10}$$

which may be integrated and simplified to yield

$$\eta_{ohm,m} = -b_m \ln \left[1 - \frac{i}{i_L} \right] \tag{11}$$

where

$$b_m = \frac{C_{H^+} F D_m}{l_m n_d} \tag{12}$$

The value of b_m represents the characteristic membrane overpotential.

The electrochemical polarization is related to entropy production, P_s [13], i.e.,

$$\eta = \frac{T \cdot P_s}{2F} \tag{13}$$

Thus, entropy production due to ohmic heating within the electrolyte becomes

$$P_s = -\frac{2F b_m}{T} \cdot \ln \left[1 - \frac{i}{i_L} \right] \tag{14}$$

Alternatively, this result can be represented in terms of exergy destruction (TP_s) due to ohmic heating. In the next section, entropy production due to concentration polarization is considered.

3. Entropy production of mass transfer in porous electrodes

Concentration polarization entails a voltage drop arising from diffusive mass transport. These voltage losses occur from diffusion of fuel/oxidant gases through the porous electrodes and mass transfer to the reaction sites. When the electrical current flows through an electrode, the partial pressure at the catalyst layer reaction site is less than the gas stream bulk pressure, thereby leading to a diffusive irreversibility (called concentration polarization). As the current increases, the electrochemical reaction rate rises and the diffusion rate becomes larger. However, the maximum diffusion rate may be less than the reaction rate. At higher current densities, this may lead to lower concentrations at a reaction site. As a result, polarization increases when the gas concentration in the electrode pores decreases, eventually producing severe polarization and limiting current density. The limiting current density refers to the current density when the cell voltage potential becomes zero. Severe voltage loss does not occur until the cell current density approaches the limiting current.

Diffusion within a porous electrode affects the catalytic reaction and it involves both ordinary and Knudsen diffusion. Ordinary diffusion occurs when the diameter of a pore is large compared to the mean free path of the molecule, while Knudsen diffusion occurs when the diameter of the pore is small, relative to the molecular mean free path. In Knudsen diffusion, molecules collide more frequently with the pore walls than other molecules. During these collisions, the pore wall instantaneously absorbs and then diffusively de-absorbs the molecules. The rates of mass transfer are impeded by these collisions with the pore walls.

The Knudsen coefficient, D_K, can be derived from kinetic theory, by means of associating the gas molecule mean free path with the pore diameter as follows [15]:

$$D_K = \frac{v \bar{r}}{6} \tag{15}$$

where v is the molecular velocity (m/s) and $\bar{r}$ is the mean pore radius (m). From kinetic theory, the velocity for round, small, straight pores can be written as

$$v = 582 \sqrt{\frac{T}{M_A}} \tag{16}$$

Thus, the Knudsen coefficient for the porous solid (component A) becomes

$$D_{Ak} = 97.0 \bar{r} \sqrt{\frac{T}{M_A}} \tag{17}$$

where M_A is the molecular mass of the porous solid.

The mean pore radius can be approximated based on the material porosity, ε_A, specific surface area of the porous solid, S_A, and the bulk density of the solid electrolyte, ρ_B, whereby

$$\bar{r} = \frac{2\varepsilon_A}{S_A \rho_B} \tag{18}$$

The effective Knudsen coefficient accounts for the tortuous path of molecular motion (rather than a radial molecular path direction) and porosity of the electrode, as diffusion only occurs within the pore space. The effective coefficient is a ratio of the solid porosity, ε, to the tortuosity, ξ, of the gas molecule path, so Eq. (17) gives

$$D_{Ak(eff)} = D_{Ak}\left(\frac{\varepsilon}{\xi}\right) \tag{19}$$

The gas binary diffusion coefficient can be approximated from Chapman–Eskog theory [15], i.e.,

$$D_{AB} = 0.0018583\left(\frac{1}{M_A} + \frac{1}{M_B}\right)^{1/2} \cdot \frac{T^{3/2}}{p\sigma_{AB}^2 \Omega_{D_{AB}}} \tag{20}$$

In this equation p is the total pressure and σ_{AB} is the average collision diameter (approximately $(\sigma_A + \sigma_B)/2$). Also, $\Omega_{D_{AB}}$ is the Lennard-Jones potential based on a collision integral. This integral cannot be determined analytically. Values of collision integrals are generally taken from published tables, due to the difficulty of calculating the integrals analytically.

Effects of intermolecular interactions are modeled in the Lennard-Jones potential and collision integral. A quantum mechanical analysis of intermolecular interactions is needed to predict changes of internal molecular states, when calculating transport properties. A quantum mechanical kinetic theory of polyatomic gases based on the Waldman–Snider equation was summarized by McCourt and co-workers [16]. Wang-Chang and Uhlenbeck [17] formulated a semi-classical kinetic theory, which allows degeneracy of rotational energy states. Therefore, it can accommodate magnetic and electric field effects on the transport properties. Unfortunately, it was only formally developed for gases with rotational degrees of freedom. In contrast, the semi-classical theory accommodates all forms of internal energy. It represents a semi-classical limit of the quantum mechanical kinetic theory.

After formulating these intermolecular interactions, the effective ordinary diffusion coefficient can be determined based on the porosity to tortuosity ratio, in a similar manner as Eq. (19), i.e.,

$$D_{AB(eff)} = D_{AB}\left(\frac{\varepsilon}{\xi}\right) \tag{21}$$

Both ordinary and Knudsen diffusion may occur simultaneously within the porous electrodes of the fuel cell. Thus, the effective total diffusion coefficient becomes

$$\frac{1}{D_{A(eff)}} = \frac{1}{D_{AB(eff)}} + \frac{1}{D_{Ak(eff)}} \tag{22}$$

or

$$\frac{1}{D_{A(eff)}} = \frac{\xi}{\varepsilon}\left(\frac{1}{D_{AB}} + \frac{1}{D_{Ak}}\right) \tag{23}$$

These results are valid for both counter-current diffusion and self-diffusion. The two mass transfer mechanisms occur within either the cathode or anode of the fuel cell. Using these equations, the combined effects of both Knudsen and ordinary diffusion on concentration polarization may be predicted. If different sized pores are highly interconnected and randomly distributed, then the path of any molecule will have a nearly equivalent resistance through the porous electrode.

4. Entropy production of anode concentration polarization

Within the anode, hydrogen migrates through the electrode by diffusion. The total flux of hydrogen can be expressed as follows,

$$J_{H_2} = -D_a \nabla C_{H_2} + X_{H_2}\delta_{H_2} J_{H_2} \tag{24}$$

where D_a is the anode diffusion coefficient and X_{H_2} is the hydrogen mole fraction. The second term on the right side represents the decrease of hydrogen flux, due to interactions with nitrogen. The diffusion ratio, δ, is given by

$$\delta_{H_2} = \frac{D_{H_2,k}}{D_{H_2,k} + D_{H_2-N_2(eff)}} \tag{25}$$

Considering 1-D diffusion, Eq. (24) becomes

$$J_{H_2} = -D_{a(eff)} \cdot \frac{dC_{H_2}}{dx} + X_{H_2}\delta_{H_2} J_{H_2} \tag{26}$$

Also, it can be shown that [15]

$$J_{H_2} = -\frac{i}{2F} \tag{27}$$

and

$$dC_{H_2} = \frac{dp_{H_2}}{RT} \tag{28}$$

Substituting Eqs. (27) and (28) into Eq. (26),

$$-\frac{i}{2F} = -\frac{D_{a(eff)}}{RT} \cdot \frac{dp_{H_2}}{dx} - X_{H_2}\delta_{H_2}\frac{i}{2F} \tag{29}$$

where

$$X_{H_2} = \frac{N_{H_2}}{N_a} = \frac{P_{H_2}}{P_a} \tag{30}$$

Rearranging and multiplying both sides by p_a,

$$\frac{dp_{H_2}}{p_a - \delta_{H_2} p_{H_2}} = \frac{RTi}{2FD_{a(eff)}p_a}dx \tag{31}$$

At the cathode surface, a boundary condition of $p_{H_2} = p_{H_2}^I$ will be applied.

Integrating Eq. (31) subject to the boundary condition,

$$\int_{p_{H_2}^I}^{p_{H_2}} \frac{dp_{H_2}}{((p_a/\delta_{H_2}) - p_{H_2})} = \int_0^{l_a} \frac{RTi\delta_{H_2}}{2FD_{a(eff)}p_a}dx \tag{32}$$

This yields the following partial pressure of hydrogen at the reaction sites,

$$p_{H_2} = \frac{p_a}{\delta_{H_2}} - \left(\frac{p_a}{\delta_{H_2}} - p^I_{H_2}\right) \cdot \exp\left(\frac{\delta_{H_2} RTil_a}{2FD_{a(eff)}p_a}\right) \quad (33)$$

where the superscript I refers to inlet conditions and

$$D_{a(eff)} = D_{H_2(eff)} = \frac{\xi_a}{\varepsilon_a}\left(\frac{1}{D_{H_2,k}} + \frac{1}{D_{H_2-N_2}}\right) \quad (34)$$

A similar result is obtained for the effective diffusivity within an SOFC (see Appendix).

The concentration polarization, η_{conc}, is the potential difference, ΔE, between the reversible voltage and the cell voltage when current flows through the circuit, i.e.,

$$\eta_{conc,a} = \Delta E = E_{rev} - E_{current} \quad (35)$$

which can be written in terms of the ideal standard potential for the chemical reaction, E^0, i.e.,

$$E_{rev} = E^0 + \frac{RT}{2F}\ln(C^I_{H_2}) \quad (36)$$

$$E_{current} = E^0 + \frac{RT}{2F}\ln(C_{H_2}) \quad (37)$$

Thus, the concentration polarization at the anode becomes

$$\eta_{conc,a} = \frac{RT}{n_e F}\ln\left(\frac{C^I_{H_2}}{C_{H_2}}\right) = -\frac{RT}{n_e F}\ln\left(\frac{p_{H_2}}{p^I_{H_2}}\right) \quad (38)$$

Substituting Eq. (33) into Eq. (38) yields the following result for a PEMFC.

$$\eta_{conc,a} = -\frac{RT}{2F}\ln\left[\left(\frac{p_a}{\delta_{H_2}} - \left(\frac{p_a}{\delta_{H_2}} - p^I_{H_2}\right) \cdot \exp\left(\frac{RT}{2F}\cdot\frac{\delta_{H_2} l_a}{D_{H_2(eff)}p_a}\cdot i\right)\right) \Big/ p^I_{H_2}\right] \quad (39)$$

This result is similar to past results derived for a solid oxide fuel cell [13], except that the coefficients, partial pressures, diffusion ratios and diffusion coefficients have changed, due to the different half-cell reactions in each type of fuel cell. Using Eq. (13), the entropy production associated with the concentration polarization becomes

$$P_{s,conc} = -R \cdot \ln\left[\left(\frac{p_a}{\delta_{H_2}} - \left(\frac{p_a}{\delta_{H_2}} - p^I_{H_2}\right) \cdot \exp\left(\frac{RT}{2F}\cdot\frac{\delta_{H_2} l_a}{D_{H_2(eff)}p_a}\cdot i\right)\right) \Big/ p^I_{H_2}\right] \quad (40)$$

This result was derived for the anode, while an analogous result can be derived for the cathode polarization, based on the previous procedure.

In addition to ohmic and concentration irreversibilities (discussed previously), the total entropy production within a fuel cell includes activation irreversibilities [15]. For a small anode thickness in a PEMFC (or a small cathode thickness in an SOFC), past data [21] has shown that voltage losses become independent of the limiting current density of the anode, i_{0a}. Thus, the anode concentration polarization decreases when the anode thickness becomes much smaller than the cathode thickness. The following TAP/TCS Model (Thin Anode for PEMFC/Thin Cathode for SOFC approximation) neglects the anode concentration polarization. Thus, the combined irreversibilities with activation polarization in the TAP/TCS Model become

$$P_s = \frac{2RT}{n_e F}\ln\left(\frac{i}{i_{0a}} + \sqrt{\frac{i^2}{i^2_{0a}} + 1}\right) + \frac{2RT}{n_e F}\ln\left(\frac{i}{i_{0c}} + \sqrt{\frac{i^2}{i^2_{0c}} + 1}\right) - \frac{2F^2 C_{H^+} D_m}{Tl_m n_d}\ln\left(1 - \frac{i}{i_L}\right) - \frac{RT}{4F}\ln\left[\left(1 - \frac{RTl_c}{8FD_{c,eff}p^I_{O_2}}i\right) \Big/ \left(1 + \frac{RTl_c}{8FD_{c,eff}p^I_{O_2}}i\right)\right] \quad (41)$$

On the right side of Eq. (41), the five terms represent the activation polarization (first and second terms; anode plus cathode), ohmic polarization (third term) and concentration polarization for the cathode (fourth term), respectively.

The previous results were derived for a PEMFC with the following anode and cathode half-cell reactions, respectively,

$$H_2(g) \Rightarrow 2H^+(aq) + 2e^- \quad \text{(anode)} \quad (42)$$

$$\tfrac{1}{2}O_2(g) + 2H^+(aq) + 2e^- \Rightarrow H_2O(l) \quad \text{(cathode)} \quad (43)$$

Different anode and cathode half-cell reactions are encountered in an SOFC, i.e.,

$$H_2(g) + O^= \Rightarrow H_2O(g) + 2e^- \quad \text{(anode)} \quad (44)$$

$$\tfrac{1}{2}O_2(g) + 2e^- \Rightarrow O^= \quad \text{(cathode)} \quad (45)$$

The previous procedures and coefficients were modified accordingly, so the TAP/TCS Model could be used to predict entropy production in both PEMFC and SOFCs. In the next section, these results will be presented and compared against past data involving cell voltage losses.

5. Results and discussion

In this section, numerical results of entropy production in a PEMFC and SOFC will be presented. Problem parameters are summarized in Table 1 and additional data was adopted from Refs. [13,14,22]. Unlike past studies of voltage losses in fuel cells, this section aims to calculate entropy production as a design parameter for improving performance of fuel cells. Fig. 2 illustrates close agreement between past data [14] and predicted results with the current TAP/TCS Model. These results provide useful validation of the TAP/TCS Model, which calculated voltage losses based on entropy production rather than polarization curves or empirical correlations [14]. An entropy based approach provides a useful method of characterizing voltage losses, as it encompasses all types of irreversible losses within a fuel cell. For example, power consumed by the blower to overcome channel friction and pressure losses of inflowing fuel comes at the expense of electrical current generated by the fuel cell, so it represents a thermofluid

Table 1
Operating conditions and problem parameters

Proton exchange membrane fuel cell	
Operating temperature, T (K)	373
Operating pressure, p (atm)	1.0
Limiting current, i_L (mA)	800
Exchange current density, i_0 (A/cm^2)	0.07
Specific surface resistance, R (Ω cm^2)	0.00003
Transfer coefficient, β	0.5
Equilibrium potential, E^0 (V)	1.167
Solid oxide fuel cell	
Operating temperature, T (K)	1073
Operating pressure, p (atm)	2.0
Electrolyte resistance, R_i (Ω cm^2)	0.139
Concentration resistance, R_{conc} (Ω cm^2)	0.31
$RT/4F$	0.02096
Exchange current density, i_0 (A/cm^2)	0.107
Effective diffusion coefficient, $D_{a,eff}$ (cm^2/s)	0.151
Cathode thickness, l_c (m)	0.00005
Porosity, ε	0.3
Tortuosity, ξ	6
Average pore radius, $\bar{r}$ (μm)	0.5
Electrolyte thickness, l_e (μm)	40.0
Anode thickness, l_a (μm)	750.0
Partial pressure ratio, p_{H_2}/p_{H_2O}	34.052

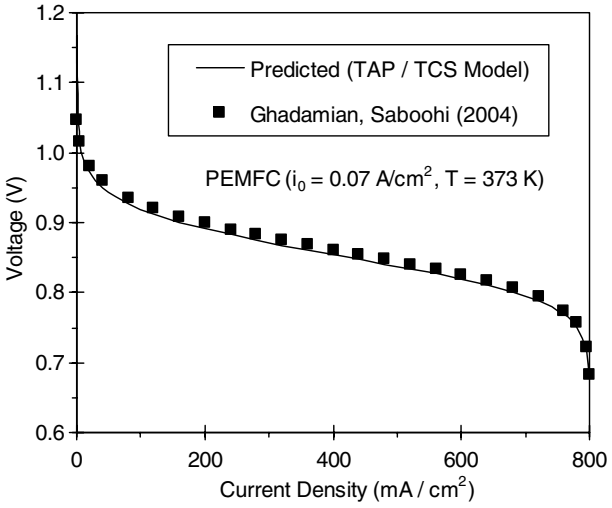

Fig. 2. Voltage profile in PEMFC ($T = 373$ K).

irreversibility that reduces the overall cell efficiency. Unlike past methods characterizing system losses through an "overpotential" or "polarization", an entropy based approach permits a more robust way of calculating all types of cell losses.

In Fig. 3, entropy production of a PEMFC is plotted at varying operational and exchange current densities (0.01, 0.04 and 0.07 A/cm^2). It can be observed that the entropy production decreases at larger exchange current densities, $i(0)$. Consider the electrode chemical activity at zero current density. Both forward and reverse reactions occur at the same rate under equilibrium, so there is forward and

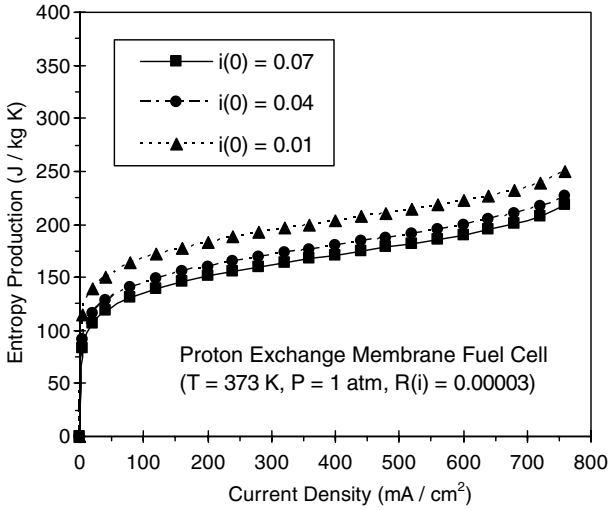

Fig. 3. Entropy production at varying current densities.

backward flow of electrons at a current density of $i(0)$. Higher exchange current densities imply more chemical activity at the electrode. The current is more likely to flow in a particular direction, so the irreversibility is reduced. Fig. 2 shows that the entropy production rises at larger operating current densities, due to larger rates of chemical reaction at the electrode surfaces and ohmic heating.

In Fig. 4, the fractions of ohmic, activation and concentration irreversibilities, relative to the total entropy production are shown as an irreversibility ratio. The respective irreversibility divided by the total entropy production represents its irreversibility ratio. For example, the activation irreversibility constitutes nearly 100% of the total entropy production at low current densities in Fig. 4, while the concentration irreversibility has rising significance at higher current densities, especially above 700 mA/cm^2. The ohmic heating irreversibility increases at larger current densities. Ohmic losses occur from electrical resistance of the

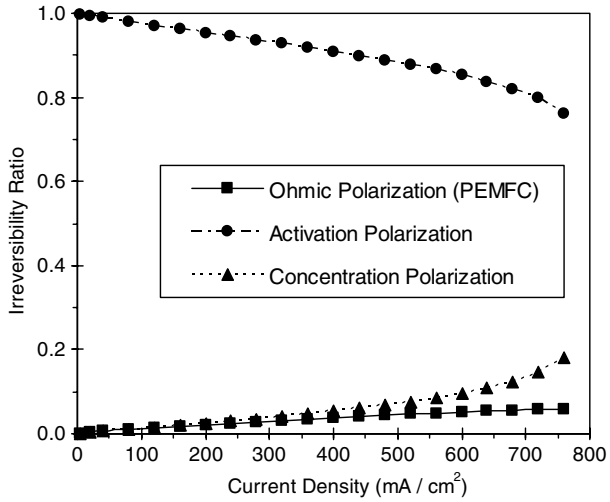

Fig. 4. PEMFC irreversibility ratio ($T = 373$ K).

electrodes, as well as resistance to ion flow in the electrolyte. Lower resistances and ohmic losses can be realized by electrodes with higher electrical conductivities. Another way is reducing the electrolyte thickness. However, this can be difficult, as it needs to be thick enough for structural support of electrodes, as well as wide enough to allow circulating flow.

An alternative method of characterizing irreversible losses is the unit irreversibility ratio, which represents the total entropy production per unit current flow (units of entropy production divided by a reference current density). Fig. 5 shows this new parameter at varying interface surface resistances of 0.00003, 0.00006 and 0.00009 $k\Omega/cm^2$. The unit irreversibility ratio rises at higher surface resistances, due to larger ohmic heating. Also, it rises fastest at low current densities due to the rapid increase of activation irreversibilities. Activation losses arise from slow reactions on the electrode surfaces. They represent a proportion of voltage lost at the electrode surface, when driving the reaction at the electrode. At higher current densities, larger activity occurs at the electrode surface and the irreversibilities rise at higher current densities. The results in Fig. 5 were obtained for a PEMFC at 373 K, while additional results show that the activation irreversibility rises less rapidly at higher operating temperatures.

Predicted results in Figs. 2–5 have used empirical diffusion coefficients based on kinetic theory and Chapman–Eskog theory discussed in Section 3. Measurements of diffusion coefficients and other transport properties in fuel cells are usually very time-consuming and expensive [18]. As a result, accurate predictive models of diffusion coefficients become necessary for fuel cell analysis. The predictive models based on statistical thermodynamics involve intermolecular interactions between gas molecules and energy exchange functions. For example, only one or a few quanta of rotational energy are exchanged in collisions between rotating molecules [19,20]. Since the rotational quantum at common operating temperatures of fuel cells is much smaller than the relative kinetic energy of a colliding pair of gas molecules, the influences of rotational energy can be neglected. For vibrational degrees of freedom, only the lowest vibrational energy states are occupied at the common operating temperatures of fuel cells.

Transport coefficients describe the process of thermodynamic relaxation to equilibrium from a state perturbed by temperature, pressure, density, velocity or composition gradients. When predicting diffusion coefficients in Section 3, kinetic theory of dilute gases assumes sufficiently low densities that molecules move freely and interact through binary collisions only. Also, the densities are high enough that molecule–wall collision effects can be neglected, relative to molecule–molecule collisions. Intermolecular exchange affects both diffusion coefficients and the resulting entropy production, due to diffusive irreversibilities of concentration polarization.

The previous figures have considered entropy production in a PEMFC. The remaining figures consider irreversibilities in SO fuel cells. In Fig. 6(a), entropy production increases at larger partial pressures of hydrogen fuel. When

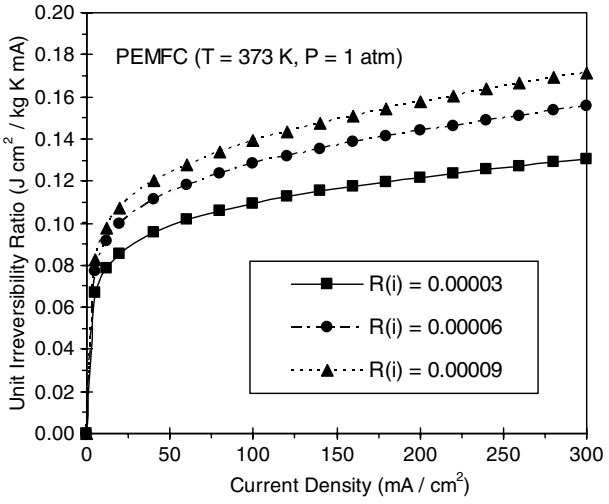

Fig. 5. PEMFC entropy production per unit current flow.

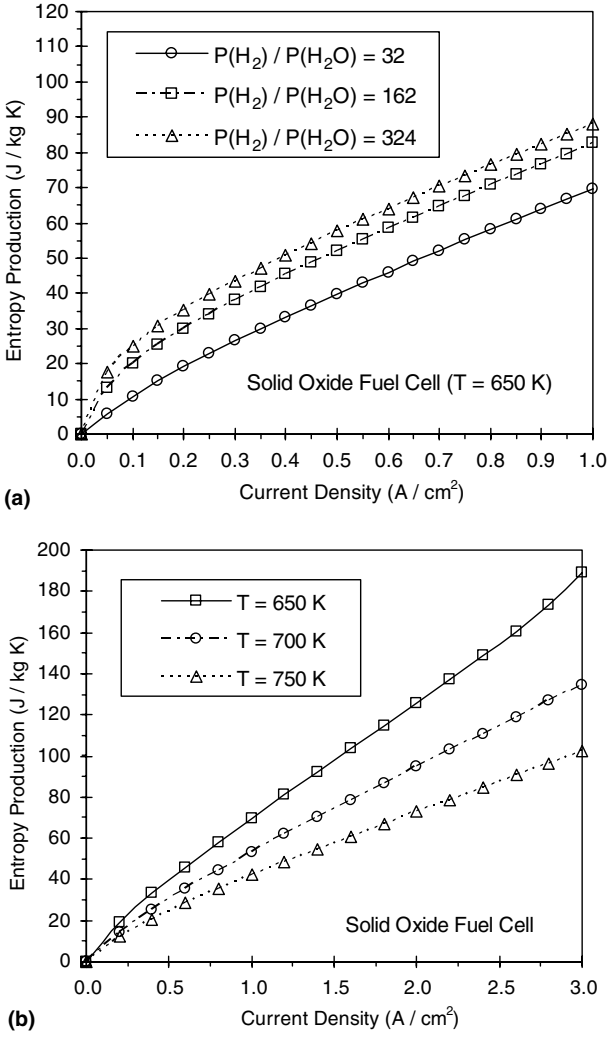

Fig. 6. Entropy production in a solid oxide fuel cell.

electric current is taken from the fuel cell, hydrogen is consumed and the operating pressure falls. Frictional resistance of hydrogen gas flowing through the fuel channels leads to a pressure loss, which depends on the operating current and hydrogen supply. This pressure reduction leads to a lower voltage. Unlike a PEMFC in Fig. 3, the total entropy production rises less rapidly at low current densities for an SOFC in Fig. 6(b). Also, higher entropy production is observed at lower operating temperatures in the SO fuel cell. The thermal conductivity usually decreases at lower temperatures. Thus, higher ohmic losses occur and SO fuel cell performance decreases when the operating temperature is lowered. An emerging area of active fuel cell research is developing better low-temperature electrodes and electrolytes, as material and construction costs are usually lower. Zirconia based electrolytes are widely used due to their favourable conductivity properties. However, Ishihara et al. [23] have developed a new oxide ion conductor, LaSrGaMgO (LSGM), which provides performance at 800 °C comparable to a YSZ (yttria-stabilized zirconia) electrolyte at 1000 °C. The composition of 8 mol YSZ is (ZrO2) 0.92 (Y2O3) 0.08, with the same crystal structure as fluorite (single phase).

Unlike loss analysis based on polarization curves, entropy production encompasses both thermofluid irreversibilities (such as friction within fuel channels) and electrochemical losses (within electrodes and electrolyte). In this way, it provides a useful parameter for purposes of systematic optimization. Differentiating the entropy production with respect to current density can identify regions having minimal changes to operating performance. For example, design changes with currents near 1.5 A/cm^2 would have least impact on voltage losses, as Fig. 7 illustrates minimal changes of entropy production near that design point. However, changes below 0.25 A/cm^2 or above 2.75 A/cm^2 would have more appreciable impact on reduced efficiency, as entropy production changes are notably larger.

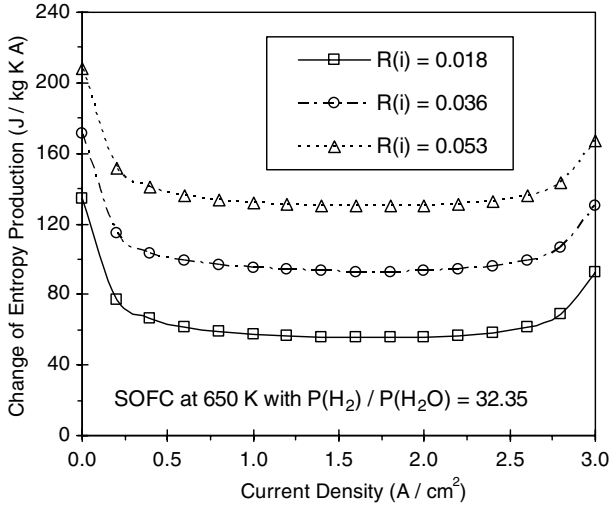

Fig. 7. Entropy production changes at varying current density.

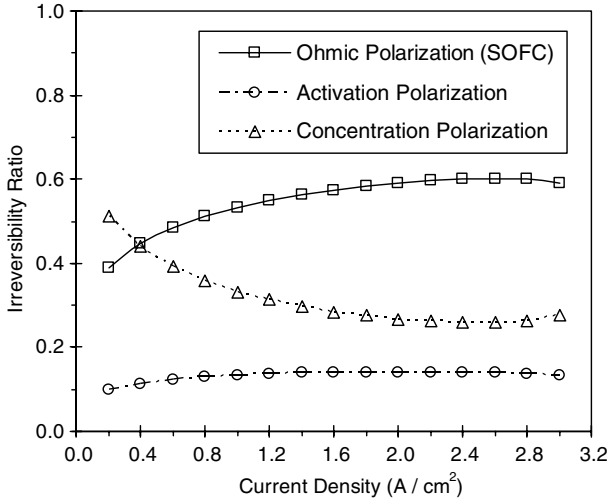

Fig. 8. SOFC irreversibility ratio.

Also, the total entropy production can be sub-divided into individual components of ohmic, activation and concentration irreversibilities (see Fig. 8). Concentration losses dominate at low current densities, but ohmic losses rise to exceed concentration irreversibilities at higher current densities. Activation irreversibilities remain nearly uniform over the range of current densities shown in Fig. 8. Fig. 9 shows the relative percentage of each irreversibility, with respect to total entropy production within the fuel cell. In comparison to a PEMFC, the higher operating temperatures of SO fuel cells reduce the relative portion of activation losses. Ohmic irreversibilites at the cathode are dominant, despite higher resistivities of the electrolyte and cell inter-connection, due to the short connection path through these components and a longer current path from the anode of one cell to the cathode of the next adjacent cell [24].

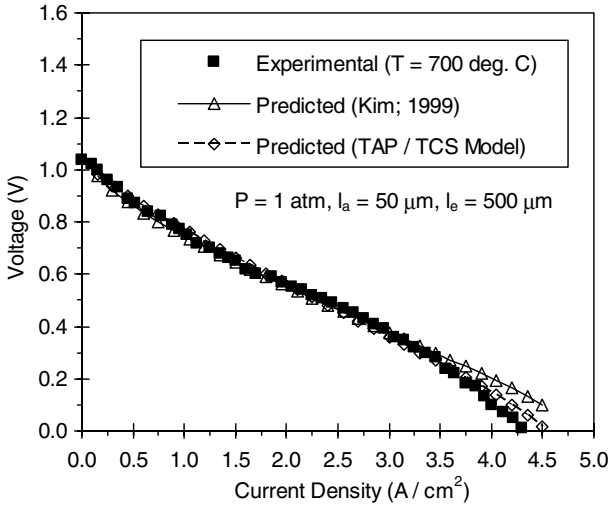

Fig. 9. Comparison of SOFC voltage profile with measured data ($T = 700$ °C).

Although it is a more general measure of thermodynamic loss, entropy production can be expressed in terms of other conventional loss parameters in a fuel cell, such as cell voltage. When re-formulated in that manner and compared against past predictions by Kim and co-workers [21], the current TAP/TCS model exhibits close agreement with measured data [13]. Slightly better accuracy is obtained with the TAP/TCS model at high operating current densities. Voltage drops at higher current densities correspond to rising entropy production in previous figures.

In summary, entropy production has provided a useful basis for calculating voltage losses and characterizing fuel cell performance. Fuel cells are complex systems involving many inputs and outputs, ranging from the cell power output, waste heat, gaseous emissions, fuel supply, blower power input and so forth. Entropy production encompasses all types of energy conversion, so it provides a robust design parameter and useful alternative to conventional loss parameters, such as polarization or overpotential.

6. Conclusions

This article has formulated entropy production of ohmic heating and concentration polarization in fuel cells. Ohmic heating of electrical resistance through the electrodes, as well as ion flow through the electrolyte, leads to irreversible losses of cell voltage. Entropy production due to resistive heating was formulated based on Ohm's law. Also, changes in reactant concentration lead to diffusive entropy production at the electrode surfaces. The predicted results have shown that entropy production rises at larger operating current densities, due to larger rates of chemical reaction at the electrode surfaces and ohmic heating. Also, the unit irreversibility ratio rises at higher surface resistances, due to larger ohmic heating. It rises fastest at low current densities due to the rapid increase of activation irreversibilities. In solid oxide fuel cells, higher entropy production was observed at low operating temperatures. In these cases, higher ohmic losses occur and fuel cell performance decreases when the operating temperature is lowered. The results have shown that entropy production provides a useful parameter for characterizing fuel cell performance. Entropy based design provides a robust alternative approach for reducing voltage losses in fuel cells.

Acknowledgements

Support of this research from the Natural Sciences and Engineering Research Council of Canada is gratefully acknowledged.

Appendix. Effective mass diffusivity of SOFC electrode

In Section 4, the effective diffusivity for a PEMFC was derived. As outlined by Eqs. (42)–(45), different anode and cathode half-cell reactions are encountered in an SO fuel cell. Thus, the procedures in Section 4 must be modified accordingly. In the case of the anode in an SO fuel cell at steady state, the reaction stoichiometry yields the following mass balance,

$$J = J_{H_2} + J_{H_2O} = 0 \tag{A.1}$$

The fluxes of hydrogen and water are given by

$$J_{H_2} = -D_{H_2(eff)} \nabla C_{H_2} + C_{H_2} v \tag{A.2}$$

$$J_{H_2O} = -D_{H_2(eff)} \nabla C_{H_2O} + C_{H_2O} v \tag{A.3}$$

where C_{H_2O} and C_{H_2} are the concentrations of water and hydrogen, respectively.

The effective total diffusion coefficients, $D_{H_2O(eff)}$ and $D_{H_2(eff)}$, are given by

$$D_{H_2(eff)} = \left(\frac{1}{D_{H_2,k}} + \frac{1}{D_{H_2-H_2O(eff)}} \right)^{-1} \tag{A.4}$$

$$D_{H_2O(eff)} = \left(\frac{1}{D_{H_2O,k(eff)}} + \frac{1}{D_{H_2-H_2O(eff)}} \right)^{-1} \tag{A.5}$$

For equimolar counter-current mass transfer in an SO fuel cell anode, the fluxes are equal so

$$J_{H_2} = -J_{H_2O} \tag{A.6}$$

Using Eqs. (A.2) and (A.3), it can be shown that

$$v = \frac{D_{H_2(eff)} - D_{H_2O(eff)}}{C_a} \cdot \nabla C_{H_2} \tag{A.7}$$

where

$$C_a = C_{H_2} + C_{H_2O} \tag{A.8}$$

Substituting Eq. (A.8) into Eq. (A.2) and re-arranging,

$$J_{H_2} = -\left[\left(\frac{C_{H_2O}}{C_a} \right) \cdot D_{H_2(eff)} + \left(\frac{C_{H_2}}{C_a} \right) \cdot D_{H_2O(eff)} \right] \nabla C_{H_2} \tag{A.9}$$

$$J_{H_2O} = -\left[\left(\frac{C_{H_2O}}{C_a} \right) \cdot D_{H_2(eff)} + \left(\frac{C_{H_2}}{C_a} \right) \cdot D_{H_2O(eff)} \right] \cdot \nabla C_{H_2O} \tag{A.10}$$

Reducing the bracketed terms and simplifying, the following results can be derived,

$$J_{H_2} = -D_{a(eff)} \cdot \nabla C_{H_2} \tag{A.11}$$

$$J_{H_2O} = -D_{a(eff)} \cdot \nabla C_{H_2O} \tag{A.12}$$

If the partial pressure change of hydrogen is assumed to be very gradual, then the difference between $D_{H_2O(eff)}$ and $D_{H_2(eff)}$ is very small, so $D_{a(eff)}$ becomes approximately constant.

Considering 1-D diffusion, the hydrogen flux becomes

$$J_{H_2} = -D_{a(eff)} \cdot \frac{dC_{H_2}}{dx} \tag{A.13}$$

Using Faraday's law and the ideal gas law,

$$\left(\frac{i}{2F} \right) = -D_{a(eff)} \cdot \frac{dp_{H_2}}{dx(RT)} \tag{A.14}$$

Re-arranging in terms of pressure and integrating,

$$\int_{p^{\mathrm{I}}_{\mathrm{H}_2}}^{P_{\mathrm{H}_2}} \mathrm{d}p_{\mathrm{H}_2} = \int_0^{l_a} \frac{iRT}{2FD_{\mathrm{a(eff)}}}\,\mathrm{d}x \tag{A.15}$$

thereby yielding

$$p_{\mathrm{H}_2} = p^{\mathrm{I}}_{\mathrm{H}_2} - \frac{RTl_a}{2FD_{\mathrm{a(eff)}}}\,i \tag{A.16}$$

Similarly for water vapour, the partial pressure becomes

$$p_{\mathrm{H_2O}} = p^{\mathrm{I}}_{\mathrm{H_2O}} + \frac{FRTl_a}{2FD_{\mathrm{a(eff)}}}\,i \tag{A.17}$$

where the effective diffusion coefficients are

$$D_{\mathrm{a(eff)}} = \left(\frac{p_{\mathrm{H_2O}}}{p_a}\right)\cdot D_{\mathrm{H_2(eff)}} + \left(\frac{p_{\mathrm{H_2}}}{p_a}\right)\cdot D_{\mathrm{H_2O(eff)}} \tag{A.18}$$

and

$$\frac{1}{D_{\mathrm{H_2(eff)}}} = \frac{\xi_a}{\varepsilon_a}\cdot\left(\frac{1}{D_{\mathrm{H_2,k}}} + \frac{1}{D_{\mathrm{H_2–H_2O}}}\right) \tag{A.19}$$

$$\frac{1}{D_{\mathrm{H_2O(eff)}}} = \frac{\xi_a}{\varepsilon_a}\cdot\left(\frac{1}{D_{\mathrm{H_2O,k}}} + \frac{1}{D_{\mathrm{H_2–H_2O}}}\right) \tag{A.20}$$

Using these results, similar procedures as Section 4 may be used to determine entropy production of concentration polarization within an SO fuel cell.

References

[1] U. Bossel, Efficiency of hydrogen fuel cell, diesel-SOFC-hybrid and battery electric vehicles, European Fuel Cell Forum, Morgenacherstrasse, Germany, 20 October 2003.

[2] M. Oszcipok, D. Riemann, U. Kronenwett, M. Kreideweis, M. Zedda, Statistic analysis of operational influences on the cold start behavior of PEM fuel cells, J. Power Sources 145 (2) (2005) 407–415.

[3] R. Xu, G.F. Naterer, Controlled interface acceleration in unidirectional solidification, Int. J. Heat Mass Transfer 47 (2004) 4821–4832.

[4] G.F. Naterer, Temperature gradient in the unfrozen liquid layer for multiphase energy balance with incoming droplets, ASME J. Heat Transfer 125 (1) (2003) 186–189.

[5] G.F. Naterer, Applying heat-entropy analogies with experimental study of interface tracking in phase change heat transfer, Int. J. Heat Mass Transfer 44 (15) (2001) 2917–2932.

[6] G.F. Naterer, Heat Transfer in Single and Multiphase Systems, CRC Press, Boca Raton, FL, 2002.

[7] T. Mennola, M. Mikkola, M. Noponen, T. Hottinen, P. Lund, Measurement of ohmic voltage losses in individual cells of a PEMFC stack, J. Power Sources 112 (1) (2002) 261–272.

[8] H.C. Liu, W.M. Yan, C.Y. Soong, F. Chen, Effects of baffle-blocked flow channel on reactant transport and cell performance of a proton exchange membrane fuel cell, J. Power Sources 142 (1–2) (2005) 125–133.

[9] S. Dutta, S. Shimpalee, J.W. Van Zee, Numerical prediction of mass-exchange between cathode and anode channels in a PEM fuel cell, Int. J. Heat Mass Transfer 44 (11) (2001) 2029–2042.

[10] G.F. Naterer, Embedded converging surface microchannels for minimized friction and thermal irreversibilities, Int. J. Heat Mass Transfer 48 (7) (2005) 1225–1235.

[11] N. Djilali, D. Lu, Influence of heat transfer on gas and water transport in fuel cells, Int. J. Therm. Sci. 41 (1) (2002) 29–40.

[12] T.C. Jen, T. Yan, S.H. Chan, Chemical reacting transport phenomena in a PEM fuel cell, Int. J. Heat Mass Transfer 46 (22) (2003) 4157–4168.

[13] S.H. Chan, Z.T. Xia, Polarization effects in electrolyte/electrode-supported solid oxide fuel cells, J. Appl. Electrochem. 32 (2002) 339–347.

[14] H. Ghadamian, Y. Saboohi, Quantitative analysis of irreversibilities causes voltage drop in fuel cell (simulation and modeling), Electrochim. Acta 50 (2004) 699–704.

[15] S.H. Chan, K.A. Khor, Z.T. Zia, A complete polarization model of a solid oxide fuel and its sensitivity to the change of cell component thickness, J. Power Sources 93 (2001) 130–140.

[16] F.R.W. McCourt, J.J. Beenakker, W.E. Köhler, I. Kuscer, Nonequilibrium Phenomena in Polyatomic Gases, Clarendon Press, London, 1990.

[17] C.S. Wang-Chang, G.E. Uhlenbeck, in: J. de Boer, G.E. Uhlenbeck (Eds.), Studies in Statistical Mechanics, vol. 5, North-Holland Publishers, Amsterdam, 1970.

[18] Y. Zhu, X. Lu, J. Zhou, Y. Wang, J. Shi, Prediction of diffusion coefficients for gas, liquid and supercritical fluid, Fluid Phase Equilibria 194 (2002) 1141–1159.

[19] J.H. Ferziger, H.G. Kaper, Mathematical Theory of Transport Processes in Gasses, North-Holland Publishing Company, London, 1972.

[20] S. Chapman, T.G. Cowling, Mathematical Theory of Non-Uniform Gases, third ed., University Press, Cambridge, 1970.

[21] J.W. Kim, A.V. Virkar, K.Z. Fung, K. Mehta, S.C. Singhal, Low temperature, high performance anode-supported solid oxide fuel cell, J. Electrochem. Soc. 146 (1) (1999) 69–78.

[22] F. Chen, Y.Z. Wen, H.S. Chu, W.M. Yan, C.Y. Soong, Convenient two-dimensional model for design of fuel channels for proton exchange membrane fuel cells, J. Power Sources 128 (2004) 125–134.

[23] T. Ishihara, H. Matsuda, Y. Takita, Doped LaGaO3 perovskite type oxide as a new oxide ionic conductor, J. Am. Chem. Soc. 116 (9) (1994) 3801–3803.

[24] J. Larminie, A. Dicks, Fuel Cell Systems Explained, John Wiley and Sons, Etobicoke, Ontario, Canada, 2003.